CLM-R283

CLM-R283

Multiphase flow simulations of shocks and detonations

Part III: Droplet laden gas flows

D. F. Fletcher
A. Thyagaraja

UK ATOMIC ENERGY AUTHORITY

Culham Laboratory

CLM-R283
MFCIWP(88)P63

Multiphase flow simulations of shocks and detonations

Part III: DROPLET LADEN GAS FLOWS

D.F. Fletcher and A. Thyagaraja
Culham Laboratory, Abingdon, Oxon., OX14 3DB

Abstract

In this paper we present an extension of the model described in parts I and II of this investigation. We have added further equations to the model to enable us to study droplet laden gas flows. Results are presented for cases with and without fragmentation and are compared with the analytic theory which is valid in the limit of small particle size.

Culham Laboratory
United Kingdom Atomic Energy Authority
Abingdon
Oxfordshire OX14 3DB
February 1988

ISBN: 0 85311 1685
C/13 Price: £5.00
Available from H.M. Stationery Office

Contents

Nomenclature	(ii)
1. Introduction	1
2. Description of the Model	1
2.1 Constitutive Relations	5
3. Computational Results	8
3.1 Equilibrium Conditions	8
3.2 Non-equilibrium Conditions	10
4. Discussion	12
Acknowledgement	13
References	14
Tables	15
Figures	

Nomenclature

c	sound speed or heat capacity of dust
c_D	drag coefficient
c_{fr}	constant in boundary layer stripping model
c_p	specific heat at constant pressure
c_v	specific heat at constant volume
e	internal energy
h	enthalpy ($= e + p/\rho$) or heat transfer coefficient
K	constant in the momentum equilibration term
L	lengthscale
$\dot{m}$	mass transfer source term
p	pressure
R	constant in temperature equilibration term
T	temperature
t	time
v	velocity
We	Weber number
x	space coordinate

Greek symbols

α	volume fraction
ρ	density
$\tilde{\rho}$	effective density ($= \alpha\rho$)
γ	ratio of specific heats
σ	surface tension
Γ	source term in length-scale equation

Subscripts

D	droplets
DG	dusty gas
E	effective fluid (gas + fragments)
F	fragments
G	gas

1. Introduction

In a series of earlier papers [1,2,3] we have described various stages in the development of a computer code, called CULDESAC, to study the detonation phase of a vapour explosion. Our previous work has been concerned with the development of an efficient numerical scheme to solve transient, one-dimensional, compressible multiphase flow equations and the application of these equations to model detonations in two component mixtures. Our study of detonations [3] showed the importance of determining the sound speed correctly in multi-component systems, since the sound speed plays a very significant role in the propagation behaviour of a detonation.

In a vapour explosion [4] melt particles are fragmented when a shock wave passes through a mixture of melt droplets and fluid, causing a differential velocity to develop between the components. The large droplets then fragment and the fragments transfer their thermal energy rapidly to a volatile liquid, causing vaporisation of this liquid, and a self-sustaining detonation may develop [4]. Thus it is important to check that our model predicts sound speeds in droplet laden flows correctly and can account successfully for fragmentation.

In this paper we describe our model and present results for droplet laden gas flows, for cases with and without particle fragmentation. In section 2 of this paper we describe the equations being solved, together with the form of the constitutive relations currently implemented in the code. In section 3 we present results obtained from our code and compare them with analytic solutions, where they are available. In section 4 we draw some conclusions and outline our plans for future work.

2. Description of the Model

We consider a gas containing large droplets of an incompressible liquid. These droplets are fragmented by the relative motion that is caused as a shock wave passes through the mixture [5]. The model has been developed in such a manner that two fundamentally different fragmentation process can be studied. The first corresponds to catastrophic breakup

which occurs at very high Weber numbers [6]. In this case the particle length-scale is diminished until the Weber number of the particles is reduced to a critical value. In the second, which corresponds to a boundary layer stripping mechanism, particles are continually stripped from the larger drops [6] and we assume that these fragments instantaneously attain thermal and mechanical equilibrium with the surrounding fluid.

Thus the model consists of 3 components: gas (G), droplets (D) and fragments (F). The following equations determine the behaviour of the system:

Conservation of Mass

$$\frac{\partial}{\partial t}(\alpha_D) + \frac{\partial}{\partial x}(V_D \alpha_D) = - \dot{m}_D \qquad \text{(Droplets)} \qquad (2.1)$$

$$\frac{\partial}{\partial t}(\alpha_F) + \frac{\partial}{\partial x}(V_G \alpha_F) = \dot{m}_D \qquad \text{(Fragments)} \qquad (2.2)$$

$$\frac{\partial}{\partial t}(\rho_G \alpha_G) + \frac{\partial}{\partial x}(V_G \alpha_G \rho_G) = 0 \qquad \text{(Gas)} \qquad (2.3)$$

Conservation of Momentum

$$\frac{\partial}{\partial t}(\alpha_D \rho_D V_D) + \frac{\partial}{\partial x}(\alpha_D \rho_D V_D^2) = - \alpha_D \frac{\partial p}{\partial x} + K(V_G - V_D) - \dot{m}_D V_D \qquad \text{(Droplets)} \qquad (2.4)$$

$$\frac{\partial}{\partial t}((\alpha_F \rho_D + \alpha_G \rho_G) V_G) + \frac{\partial}{\partial x}((\alpha_F \rho_D + \alpha_G \rho_G) V_G^2)$$

$$= - (\alpha_F + \alpha_G) \frac{\partial p}{\partial x} + K(V_D - V_G) + \dot{m}_D V_D \qquad \text{(Gas + Fragments)} \qquad (2.5)$$

Conservation of Energy

$$\frac{\partial}{\partial t}\left(\rho_D \alpha_D \left(e_D + \frac{1}{2} V_D^2\right)\right) + \frac{\partial}{\partial x}\left(\rho_D \alpha_D V_D \left(h_D + \frac{1}{2} V_D^2\right)\right)$$

$$= - p \frac{\partial \alpha_D}{\partial t} + R(T_C - T_D) - \dot{m}_D \left(h_D + \frac{V_D^2}{2}\right)$$

$$+ V_D K(V_G - V_D) \qquad \text{(Droplets)} \tag{2.6}$$

$$\frac{\partial}{\partial t}\left(\rho_D \alpha_F \left(e_F + \frac{1}{2} V_G^2\right) + \rho_G \alpha_G \left(e_G + \frac{1}{2} V_G^2\right)\right)$$

$$+ \frac{\partial}{\partial x}\left(V_G \left(\rho_D \alpha_F \left(h_F + \frac{1}{2} V_G^2\right) + \rho_G \alpha_G \left(h_G + \frac{1}{2} V_G^2\right)\right)\right)$$

$$= - p \frac{\partial \alpha_G}{\partial t} - p \frac{\partial \alpha_F}{\partial t} + R(T_D - T_C) + \dot{m}_D \left(h_D + \frac{V_D^2}{2}\right)$$

$$+ V_G K(V_D - V_G) + K(V_D - V_G)^2 \quad \text{(Gas + Fragments)} \tag{2.7}$$

In addition we have

$$\alpha_F + \alpha_G + \alpha_D = 1 \tag{2.8}$$

The droplet length-scale is determined from

$$\frac{\partial}{\partial t}(\alpha_D L_D) + \frac{\partial}{\partial x}(\alpha_D V_D L_D) = - \dot{m}_D L_D + \Gamma \tag{2.9}$$

where Γ is the fragmentation source term (described in Section 2.1).

We also have the following equations of state

$$\rho_D = \rho_F = \text{constant} \tag{2.10}$$

$$e_D = c_{vD}\, T_D \tag{2.11}$$

$$e_F = c_{vD}\, T_G \tag{2.12}$$

$$p = p_G\, c_{vG}\, (\gamma_G - 1)\, T_G \tag{2.13}$$

and $$e_G = c_{vG}\, T_G \tag{2.14}$$

At this stage we will make a few comments on the above system of equations:

(i) The mass conservation equations for the droplets and fragments provide a simple means of time advancing the volume fraction of each species. Equation (2.3) can then be time advanced to obtain $\rho_G \alpha_G$ and α_G and ρ_G can be obtained using equation (2.8).

(ii) The momentum equations are very similar to those used in our previous work. The equation for the gas and fragments was obtained by summing the respective momentum equations and putting the two velocities equal. These equations were time advanced exactly as before.

(iii) Both energy equations are written in stagnation form and the energy equation for the gas and fragments was obtained by summing the respective energy equations and setting their velocities and temperatures to a common value. If the two remaining energy equations are summed all the source terms vanish and the total energy of the system is conserved. We have chosen to add all the irreversible work arising from drag and mass transfer to the gas phase equation. In the present model the volume fractions can be obtained directly from the mass conservation equations so that the pressure work terms can be centre-differenced in time.

(iv) The pressure is obtained using equation (2.13) after the temperatures have been obtained from the internal energies using equations (2.11), (2.12) and (2.14). Note that because the droplets are assumed to

be incompressible the properties of the droplets play no part in determining the pressure field. In the present work we have used an ideal gas EOS but there is no reason why other equations of state could not be used.

We employ exactly the same solution procedures as in our earlier work except that we take advantage of the fact that the volume fractions can be determined from equations (2.1), (2.2) and (2.8) above. The length-scale equation is time advanced in exactly the same manner as that described in reference 7. We will now turn our attention to determining suitable forms for the constitutive relations.

2.1 Constitutive Relations

To close the model we have to provide expressions for the drag and temperature relaxation terms, and the particle fragmentation rate. If the volume fraction of droplets is α_D there are $6\alpha_D/\pi L_D^3$ spherical droplets per unit volume. The drag force on a single droplet may be written as

$$F_D = \frac{1}{2} c_D \rho_E \pi \frac{L_D^2}{4} |V_D - V_G| (V_G - V_D) \qquad (2.15)$$

where

$$\rho_E = \alpha_G \rho_G + \alpha_F \rho_F \qquad (2.16)$$

is the effective density of the fluid which is dragging the drops. Thus the total drag force is

$$F_T = \alpha_D \frac{3}{4} \frac{c_D \rho_E}{L_D} |V_D - V_G| (V_G - V_D) \qquad (2.17)$$

and comparison of equation (2.17) with the RHS of equation (2.4) gives

$$K = \frac{3}{4} \alpha_D c_D \frac{\rho_E}{L_D} |V_D - V_G| \qquad (2.18)$$

In the present work we have used a constant value for c_D although it is a simple matter to make c_D a function of, for example, the droplet volume fraction as described in reference 8.

Similarly if the heat transfer rate is specified as the product of a heat transfer coefficient and the temperature difference between the droplets and gas we obtain

$$R = 6\alpha_D \frac{h}{L_D} \tag{2.19}$$

where h is an appropriate heat transfer coefficient. We have chosen to specify a constant value for h in the present study although it could easily be modified to account for the specific situation of interest, for example, it could be convective heat transfer or convective film boiling.

To simulate catastrophic breakup we set both $\dot{m}_D$ and Γ to zero. At the beginning of each timestep the Weber number, a dimensionless measure of the ratio of the destabilising force due to relative velocity effects to the stabilising effect of surface tension, was determined. If the value of the Weber number was below a critical value (We_{crit}) the length-scale was not changed. If it was not, the length-scale was reduced so that $We = We_{crit}$. The Weber number is defined as

$$We = \frac{\rho_G (V_G - V_D)^2 L_D}{\sigma_D} \tag{2.20}$$

so that we set

$$L_D = \frac{\sigma_D We_{crit}}{\rho_G (V_G - V_D)^2} \tag{2.21}$$

for $We > We_{crit}$ and equation (2.9) was then used to track the particle lengthscale. This model assumes instantaneous breakup but could easily be modified to allow for a finite fragmentation rate. This has not been done as a boundary layer stripping model is thought to be more appropriate to vapour explosions [9].

The boundary layer stripping model used in this work is the same as that developed by Carachalios et al. [9]. They suggest that the mass stripping rate from a single fragment is given by

$$\frac{dm}{dt} = c_{fr} \left|V_D - V_G\right| \pi L_D^2 \left(\rho_D \rho_E\right)^{1/2} \qquad (2.22)$$

where $c_{fr} \sim \frac{1}{6}$. Multiplying equation (2.22) by the number of drops per unit volume and comparing the result with equation (2.1) gives

$$\dot{m}_D = \alpha_D c_{fr} \frac{\left|V_D - V_G\right|}{L_D} \left(\rho_E / \rho_D\right)^{1/2} \qquad (2.23)$$

where all the constant terms have been included in c_{fr} so that $c_{fr} \sim 1$. Equation (2.23) predicts that the breakup rate is proportional to the relative velocity, the square root of the effective fluid to droplet density ratio and inversely proportional to the droplet diameter. These are the convential quantities used to non-dimensionalise breakup time data [6]. As fragmentation occurs, the density of the surrounding fluid is increased by the addition of fragments and thus the fluid has more inertia to fragment the drops.

The length-scale of the droplets is changed by the mass loss due to boundary layer stripping. For spherical drops it is easily shown that the mass stripping rate given by equation (2.22) implies a length-scale source term given by:

$$\Gamma = -\frac{1}{3} \dot{m}_D L_D \qquad (2.24)$$

which is not surprising, as equation (2.24) implies that a droplet's length-scale changes at one third the rate of its volume. No information is required about the size of the fragments since these are assumed to equilibriate their velocity and temperature instantaneously with the surrounding fluid.

We have added a modification of our own to the above boundary layer stripping formula to ensure that as the Weber number falls to a value of 12 breakup is terminated. Boundary layer stripping occurs for the Weber

number range $100 \leqslant We \leqslant 350$ [6]. For Weber numbers below this some small fragments are produced due to bag and bag-and-stamen breakup. Thus we introduced the following simple function to multiply the constant c_{fr} in equations (2.23) and (2.24)

$$f(We) = 0 \qquad We \leqslant 12$$
$$= 1 - \exp(-(We-12)/20) \qquad We > 12 \tag{2.25}$$

This function ensures that stripping is gradually decreased from We = 100 to We = 12. Clearly any simple prescription could be used and the above expression could be modified if improved data becomes available.

This now constitutes a complete description of the model and we will present some results in the next section.

3. Computational Results

In this section we present the results obtained from the model described in the previous section. We have used the code to model droplet laden gases with and without droplet fragmentation. The test cases described in this paper are based on similar test cases performed by Jones and Jones [10].

3.1 Equilibrium Conditions

If the droplets are very small they will have the same velocity and temperature as the gas at all times. In this case there is a well-established theory of the behaviour of dusty gases [11]. A mixture of dust particles and gas can be modelled as an ideal gas with modified properties. The density of the gas is given by

$$\rho_{DG} = \alpha_G \rho_G + \alpha_D \rho_D \tag{3.1}$$

and the modified ratio of specific heats is given by

$$\gamma_{DG} = \frac{c_{pG} + \kappa c}{c_{vG} + \kappa c} \tag{3.2}$$

where $\kappa = \frac{\alpha_D \rho_D}{\alpha_G \rho_G}$ (3.3)

and c is the heat capacity of the gas. The modified sound speed in the gas is given by

$$c_{DG}^2 = \frac{c_D^2 \gamma_{DG}}{\gamma_G (1+\kappa)} \quad (3.4)$$

This equation shows that the presence of dust can effect the sound speed significantly, since for large dust fractions $\gamma_{DG} \sim 1$ and c_{DG} is reduced because of the $1 + \kappa$ factor in the denominator. Physically, the reduction in sound speed occurs because of the greater inertia of the gas.

We have carried out a number of calculations to examine the behaviour of our model in this situation. Our starting point was to repeat the shock tube calculation reported in reference 1 to provide a base case calculation. The parameters used in the calculation are given in Table 1.

The calculation was then repeated with a 1 kg/m^3 of dust added to the gas. The properties of the dust are given in Table 2. Equations (3.1) and (3.2) were used to calculate the analytic solution to the problem in the same manner as described in reference 1. The same calculation was carried out using two different routes. In the first, the dust was treated as fragments in equations (2.1) - (2.14), so there was no need to specify a particle size and by construction the dust and gas had the same velocity and temperature. In the second, the dust was treated as droplets with a very small size (10 μm) and the drag and temperature relaxation rates were set to a high value. Both solutions were found to be in good agreement with the analytic theory (which is in good agreement with experimental data [11]) and with each other.

Figures 1(a), (b), (c) and (d) show a comparison of the computed pressure, velocity, temperature and density with the analytic solution (obtained using the first method). Agreement is seen to be very good with no overshoots at the shock front. The density and temperature solutions

are slightly smeared by the numerical method but the results are good considering the coarseness of the grid. We have carried out a fine grid simulation, using 800 grid points, to demonstrate the consistency and convergence of the numerical scheme. The fine grid solution for the density is given in figure 1(d) and shows that the numerical diffusion is considerably reduced. Comparison of these results with those obtained in our earlier study shows that both the shock front and the rarefaction wave are moving much more slowly in the case of a dusty gas.

We repeated the above calculation with the dust density increased by a factor of ten. The calculated pressure and velocity fields are compared with the analytic solution in figures 2(a) and (b). Again there is good agreement between the analytic and computed results. Comparison of figures 1(a) and 1(b) with figures 2(a) and 2(b) show that the presence of the dust causes an increased pressure jump at the shock front and slows down the motion of the system significantly. These test cases provided a good check of most of the features of the code. In the next section we will examine the effect of introducing slip between the drops and the gas and the effect of fragmentation.

3.2 Non-equilibrium Conditions

If the droplet size is increased the droplets and the gas can move at different speeds and have different temperatures. We have carried out a simulation for the same initial conditions as used above but where the droplets had a diameter of 1mm and no breakup was allowed. The other properties used in the simulation are given in Table 3. Figures 3(a), (b) and (c) show the pressure, velocity and temperature fields as a function of distance for the same time as for the previous examples. The equilibrium theory analytic solution is also shown for comparison purposes.* The figures show that there is no longer a steep pressure front and that the droplets and gas have different velocities and temperatures. These differences can be reduced by decreasing the particle size or increasing the drag coefficient and heat transfer coefficient. The results show that the droplets are accelerated less than the gas by

---

* Note that the analytic solution is no longer an exact solution of the problem under non-equilibrium conditions but serves as an approximate guide.

the shock wave. Also the gas is heated by the shock and cooled in the rarefaction wave whereas the droplets change their temperature very little.

We repeated the above calculation with the particle size determined by instantaneous breakup to a lengthscale determined from a critical Weber number of 12. The drag coefficient was not changed, although it should be increased when fragmentation occurs [6]. (It was kept fixed here so that only one quantity at a time was varied.) Figures 4(a), (b), (c) and (d) show the pressure, velocity, temperature and droplet diameter as a function of distance for the above case. The figures show that breakup at the shock front reduces the relative velocity between the gas and droplets and brings the solution closer to that predicted by the equilibrium theory. The breakup results in higher heat transfer rates and a reduction in the temperature difference between the droplets and the gas. Figure 4(d) shows that these droplets are fragmented from 1mm to 0.2mm in a very short distance behind the shock. Breakup is less rapid across the rarefaction wave with an initial reduction in particle size to 0.6mm followed by an extended region of further fragmentation which produces 0.2mm diameter droplets.

In the final test case the boundary layer stripping model was used. Figures 5(a), (b), (c), (d), (e) and (f) show the pressure, velocity, temperature, droplet diameter, fraction of the drops fragmented and Weber number as a function of distance. Figure 5(a) shows that the pressure profile is very similar to that produced in the case of a dusty gas. This is because droplet fragmentation is very rapid in the regions of the shock and expansion wave. Figure 5(b) shows that the velocity is equilibrated more rapidly in this case compared with the previous case. This is because the effective fluid causing breakup has an increased density, due to the presence of the fragments, resulting in a high drag force between the species and smaller drops for the same critical Weber number. Figure 5(d) shows that there is rapid fragmentation at the shock front and the rarefaction wave. The droplet diameter plot shows a region of larger diameters in the zone close to the contact surface. This region contains the droplets that were close to the contact zone originally where the relative velocity was less. This region is of very little physical

significance since figure 5(e) shows that in this region virtually all the droplets have been fragmented. Figure 5(f) shows a plot of the Weber number against distance. The plot indicates that the Weber number is increased above the critical Weber number at the shock front and at the head of the expansion fan. Between these zones the Weber number is decreased both by fragmentation, until the critical Weber number is reached, and then still further by drag as the relative velocity is reduced to zero in some places.

Comparison of the three different cases presented above shows that fragmentation changes the solution considerably. Reducing the particle size causes an increase in the drag between the droplets and the gas, which reduces the relative velocity and the solution becomes closer to that for a dusty gas. Boundary layer stripping increases this effect because the fragments increase the inertia of gas causing even lower relative velocities. Thus the choice of fragmentation model changes the sound speed in the mixture (since this depends on the relative velocity, particle size etc.) and will effect the propagation behaviour of detonations.

The results presented in this section show that the code gives results in good agreement with the analytic solution for the case of very small particles. For larger particles the code gives physically sensible results which are in qualitative agreement with those of Jones and Jones [10].

4. Discussion

In this paper we have described the mathematical framework of our proposed model of the detonation stage of a vapour explosion. We have used this model to examine droplet laden gas flows for cases with and without droplet fragmentation. Our results are in good agreement with analytic theory and previous work.

The next stage in the development of our detonation model is to replace the ideal gas equation of state with one suitable for water. The model could then be used to examine fragmentation and detonations in melt/water mixtures.

Acknowledgement

The authors would like to thank Mrs.E.Barnham for her careful preparation of this manuscript.

References

1. Fletcher, D.F. and Thyagaraja, A., Some calculations of shocks and detonations for gas mixtures. Culham Laboratory Report: CLM-R276, (1987).
2. Fletcher, D.F. and Thyagaraja, A., Multiphase flow simulations of shocks and detonations. Part I: Mathematical formulation and shocks. Culham Laboratory Report: CLM-R279, (1987).
3. Thyagaraja, A. and Fletcher, D.F., Multiphase flow simulations of shocks and detonations Part II: Detonations. Culham Laboratory Report: CLM-R280, (1987).
4. Board, S.J., Hall, R.W. and Hall, R.S., Detonation of fuel coolant explosions. Nature, 254, 319-321, (1975).
5. Simpkins, P.G., and Bales, E.L., Water-drop response to sudden accelerations. J.Fluid Mech., 55, 629-639, (1972).
6. Pilch, M. and Erdman, C.A., Use of breakup time data and velocity history data to predict the maximum size of stable fragments for acceleration-induced breakup of a liquid drop. Int. J. Multiphase Flow, 13 , 741-757, (1987).
7. Fletcher, D.F., and Thyagaraja, A., Numerical simulation of two-dimensional transient multiphase mixing. Proc. 5th Int. Cont. on Numerical Methods in Thermal Problems, Montreal, Canada, June 29th-July 3rd, 1987, V(2), 945-956, Pineridge, (1987).
8. Ishii, M. and Zuber, N., Drag coefficients and relative velocity in bubbly, droplet or particulate flows. AIChEJ, 25, 843-855, (1979).
9. Carachalios, C., Burger, M. and Unger, H., A transient two-phase model to describe thermal detonations based on hydrodynamic fragmentation. Paper presented at Int. meeting on LWR severe accident evaluation, Cambridge, Massachusetts. August 28- September 1, (1983).
10. Jones, I.P. and Jones A.V., The numerical solution of simple one-dimensional multi-phase flows in shock tubes. Paper presented at Second Int. Conf. Numerical Methods in Laminar and Turbulent Flow, Venice, 13-16 July, (1981).
11. Marble, F.E., Dynamics of dusty gases. Ann. Rev. Fluid Mech., 2, 397-446, (1970).

High Pressure Section

$p = 2\text{MPa},$

$T = 413\text{K},$

$\rho_G = 10.7\ \text{kg/m}^3$

Low Pressure Section

$p = 0.1\text{MPa},$

$T = 300\text{K},$

$\rho_G = 0.738\ \text{kg/m}^3$

Gas properties

$c_{vG} = 1355\ \text{J/kgK},$

$\gamma_G = 1.333$

General

Length of shock tube = 73m

Position of diaphragm = 36.5m

Number of grid points = 80

Time step = 20 μs

Comparison time = 0.05s

Table 1 : Data for the shock tube calculation.

Specific heat of dust = 1300 J/kgK

Density of dust = 705 kg/m^3

(Increased to 7050 kg/m^3 in second calculation)

Volume fraction of dust = 0.001418

Table 2 : Properties of the Dust.

Diameter of droplets = 1 mm

Mass density of droplets = 705 kg/m^3

Surface Tension = 0.4 N/m

Drag Coefficient = 0.4

Heat transfer coefficient = 1000 W/m^2K

Critical Weber number = 12

Constant in boundary layer stripping model, c_{fr} = 1.0

Table 3: Properties used in large droplet simulations.

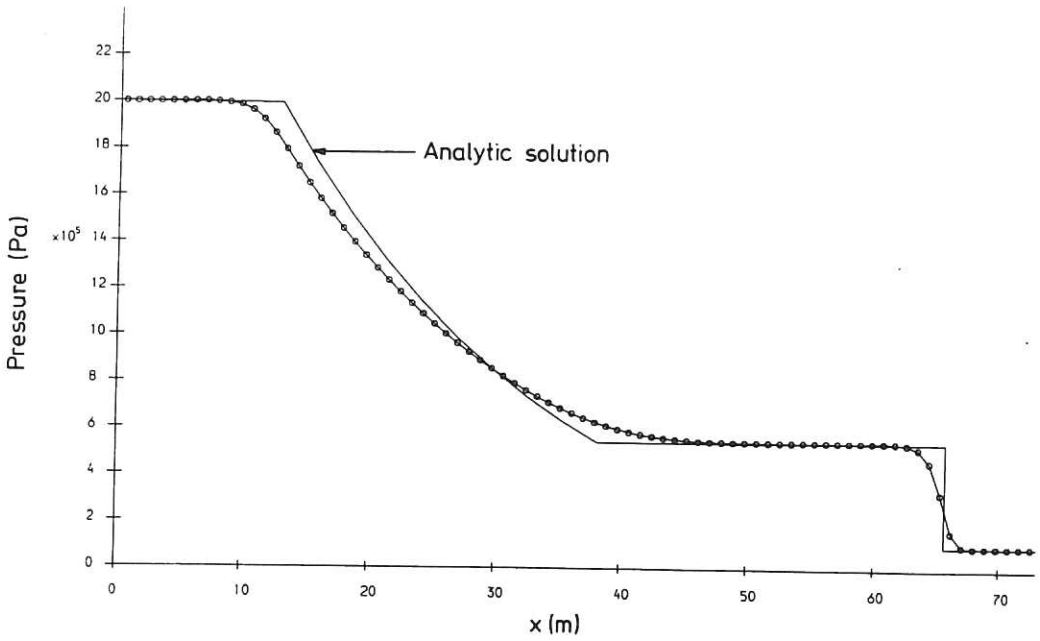

Fig.1(a): Pressure against distance for dusty gas simulation

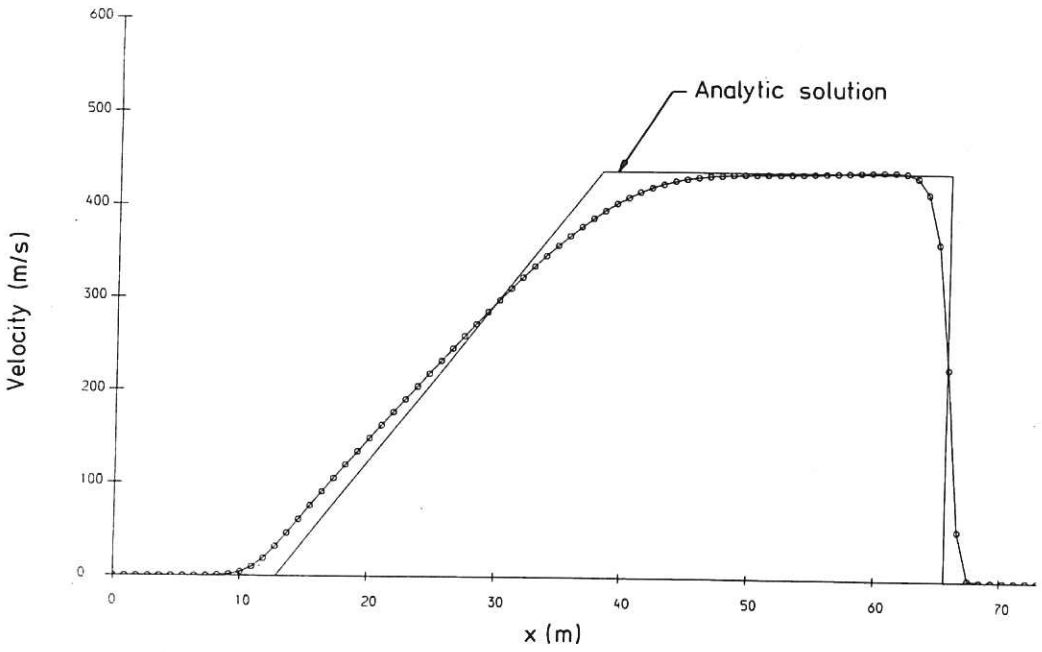

Fig.1(b): Velocity against distance for dusty gas simulation

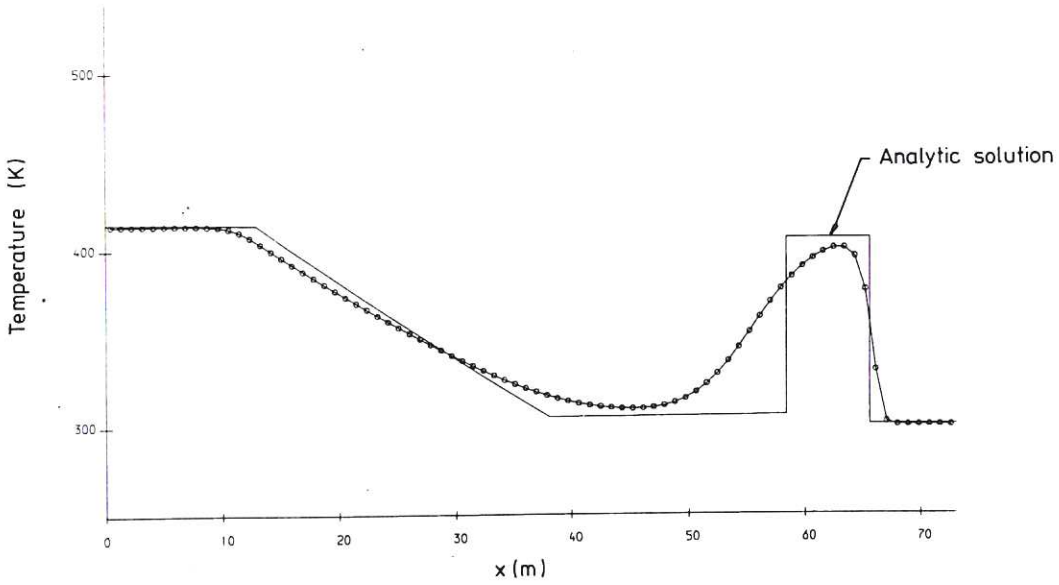

Fig.1(c): Temperature against distance for dusty gas simulation

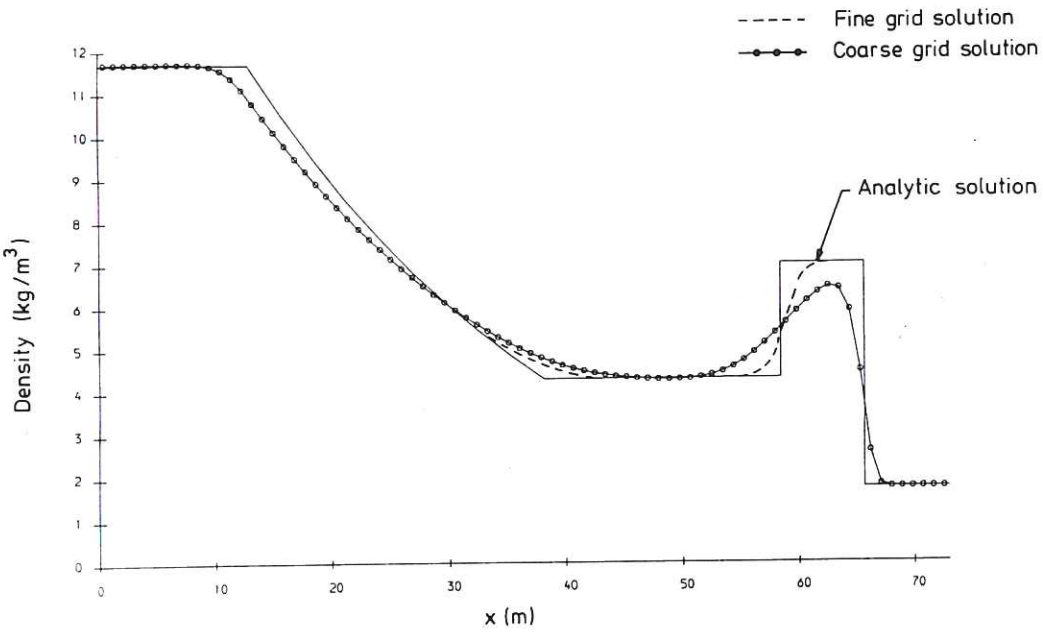

Fig.1(d): Total density against distance for dusty gas simulation

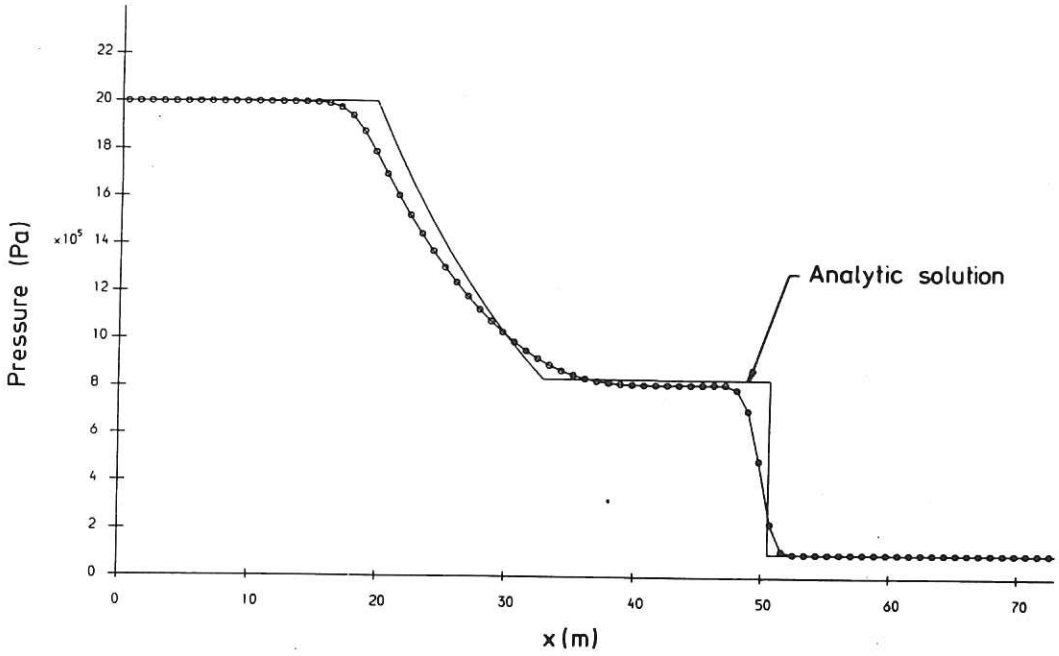

Fig.2(a): Pressure against distance for dusty gas simulation (Increased dust density)

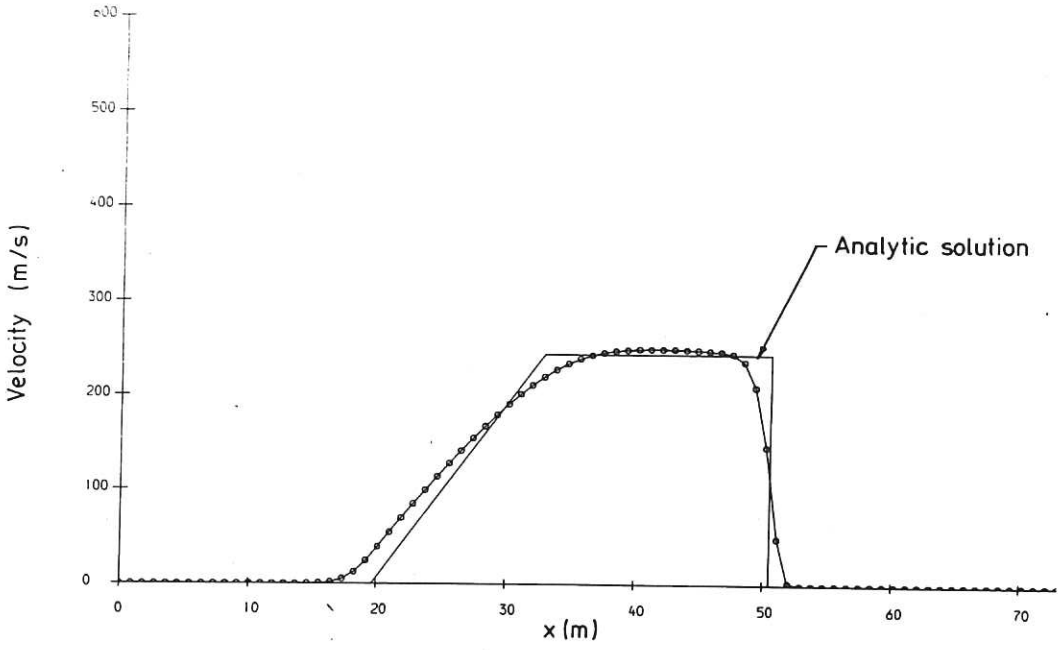

Fig.2(b): Velocity against distance for dusty gas simulation (Increased dust density)

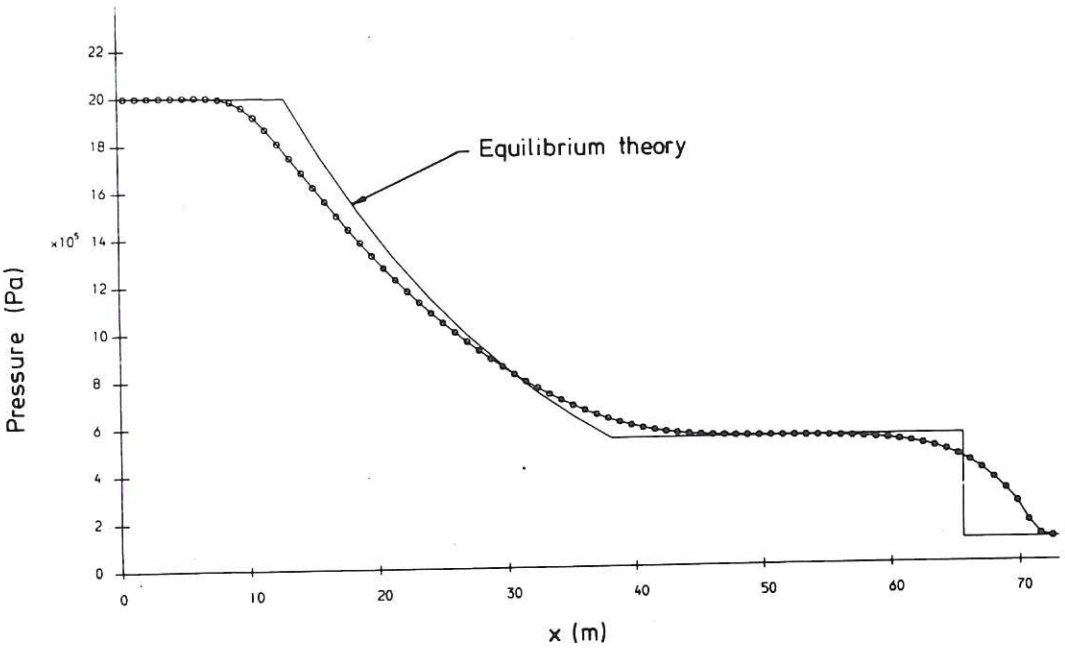

Fig.3(a): Pressure against distance for 1mm droplet case

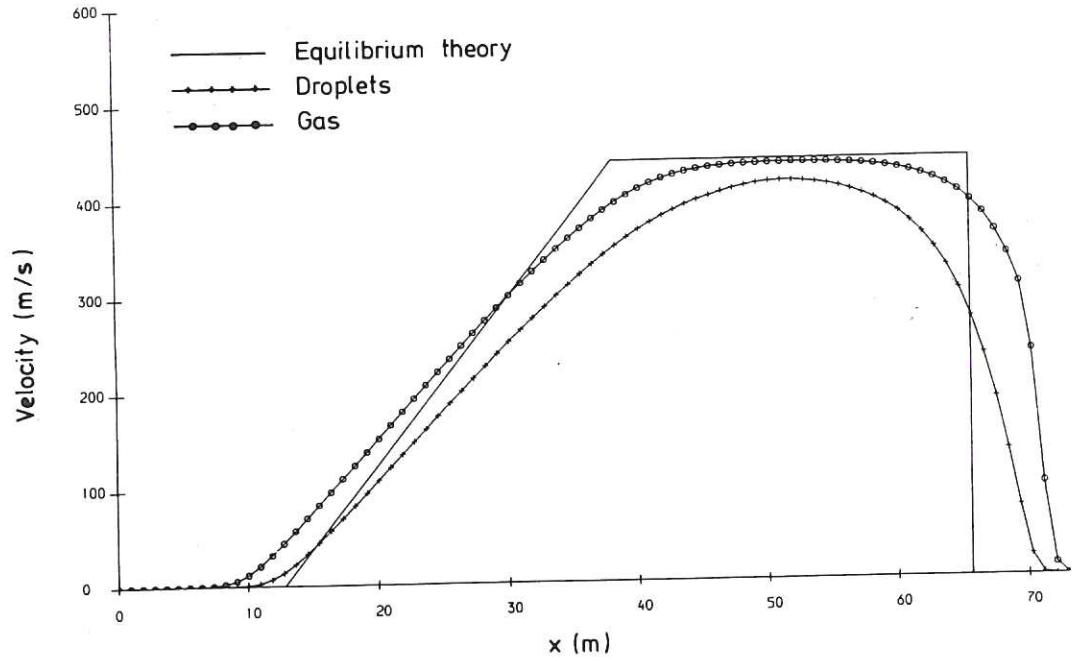

Fig.3(b): Velocity against distance for 1mm droplet case

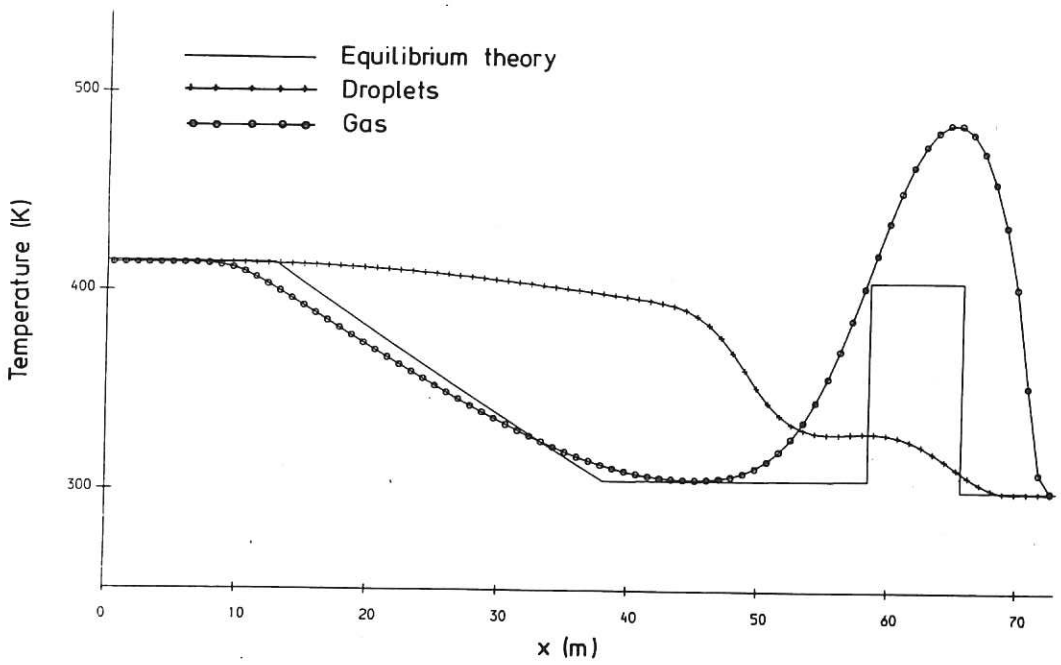

Fig.3(c): Temperature against distance for 1mm droplet case

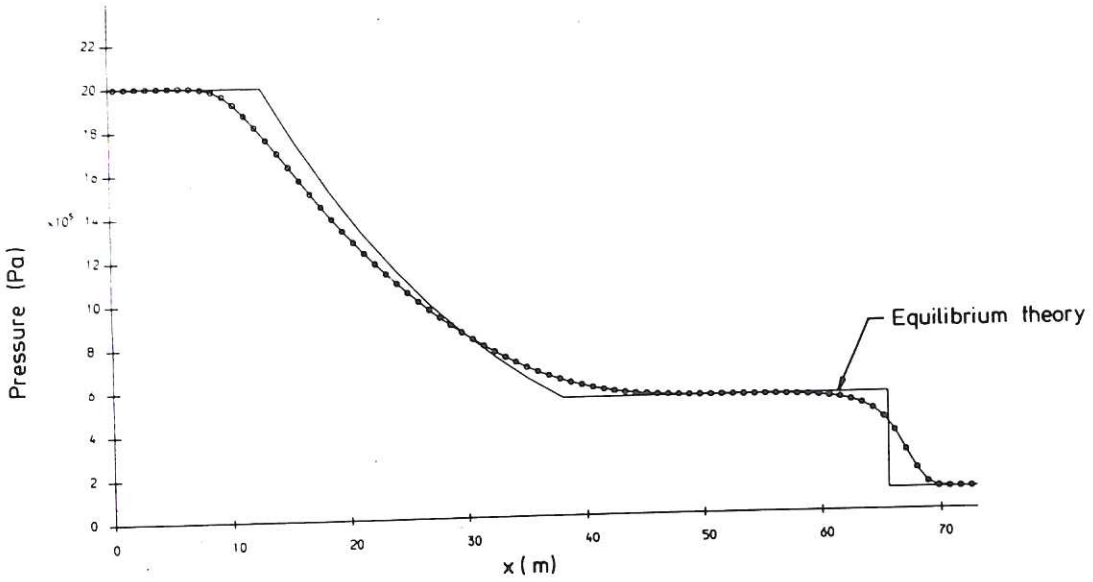

Fig.4(a): Pressure against distance for instantaneous breakup case

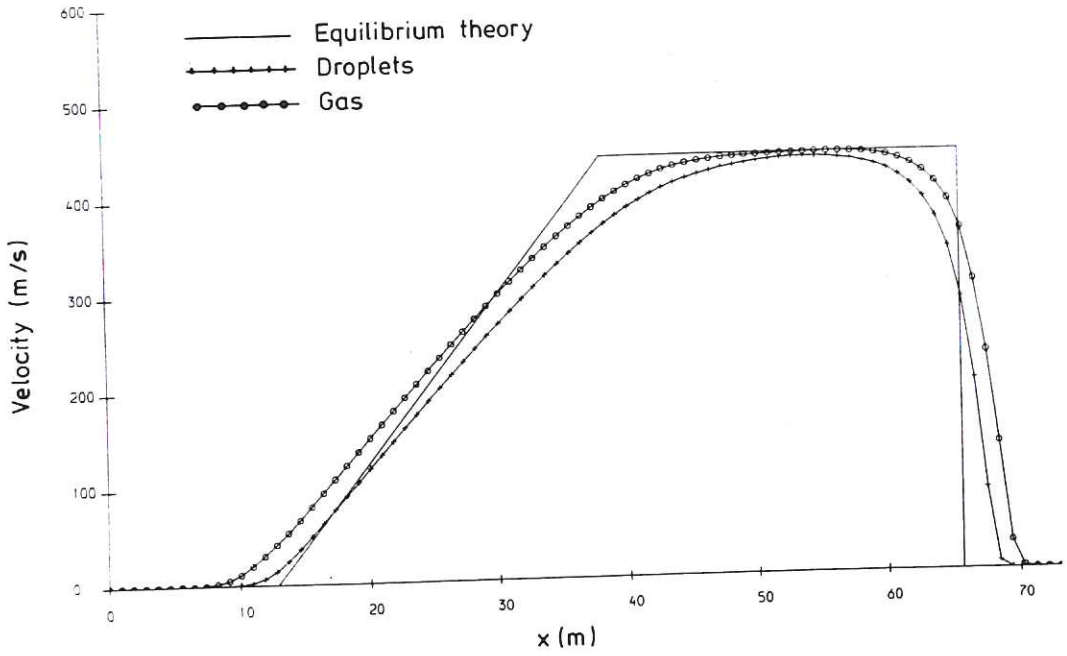

Fig.4(b): Velocity against distance for instantaneous breakup case

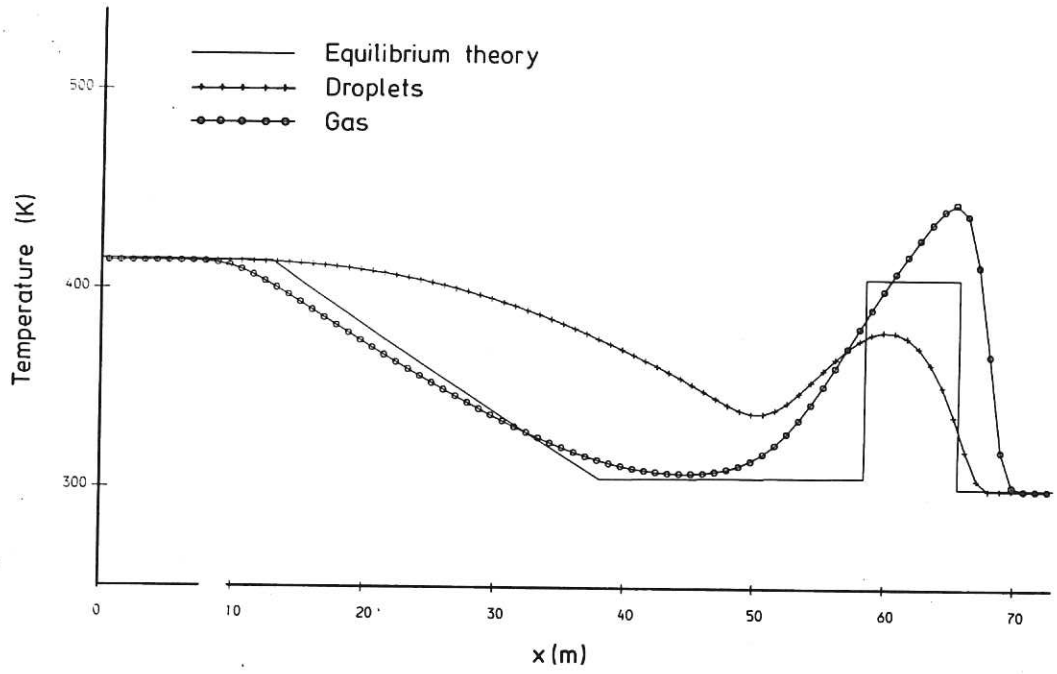

Fig.4(c): Temperature against distance for instantaneous breakup case

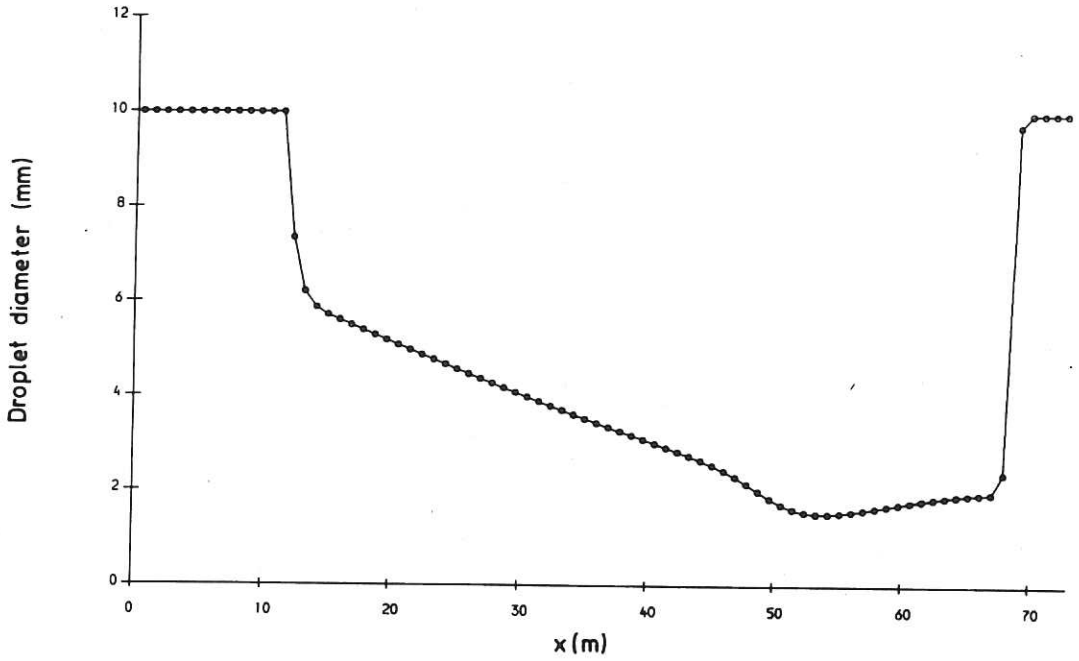

Fig.4(d): Droplet diameter against distance for instantaneous breakup case

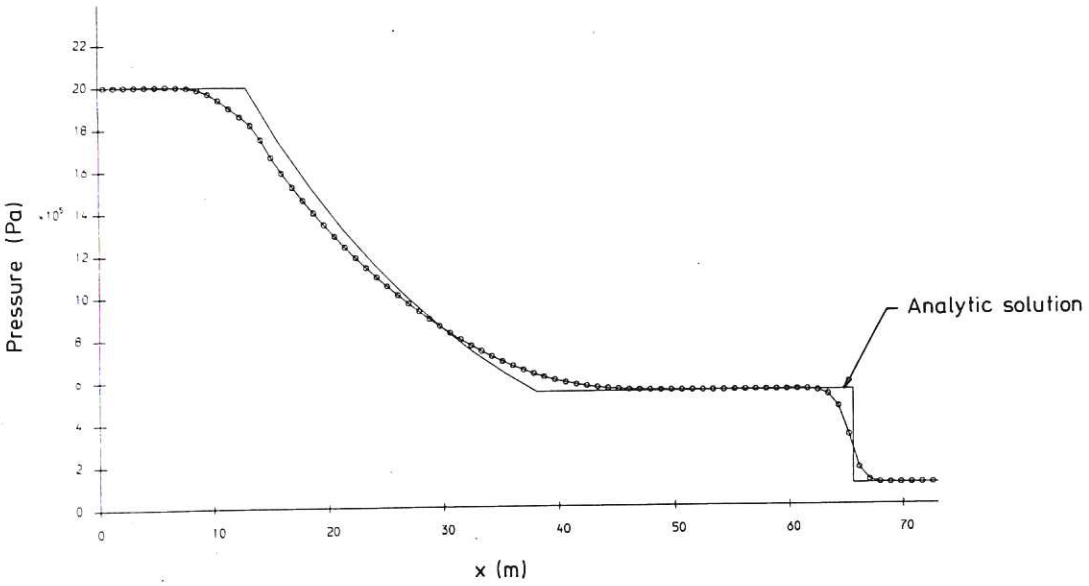

Fig.5(a): Pressure against distance for boundary layer stripping case

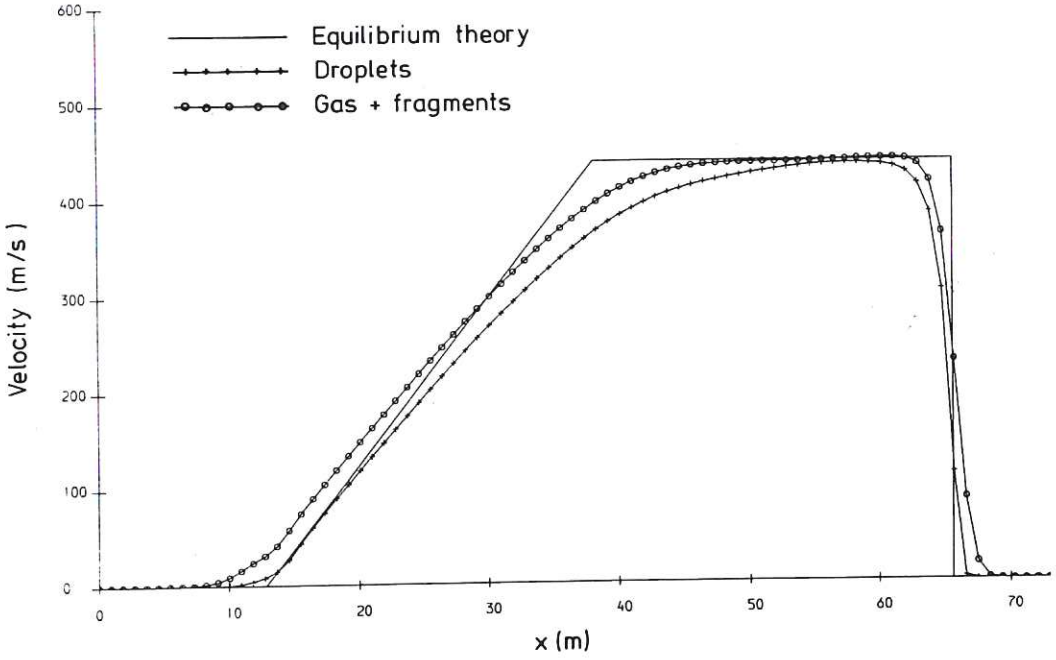

Fig.5(b): Velocity against distance for boundary layer stripping case

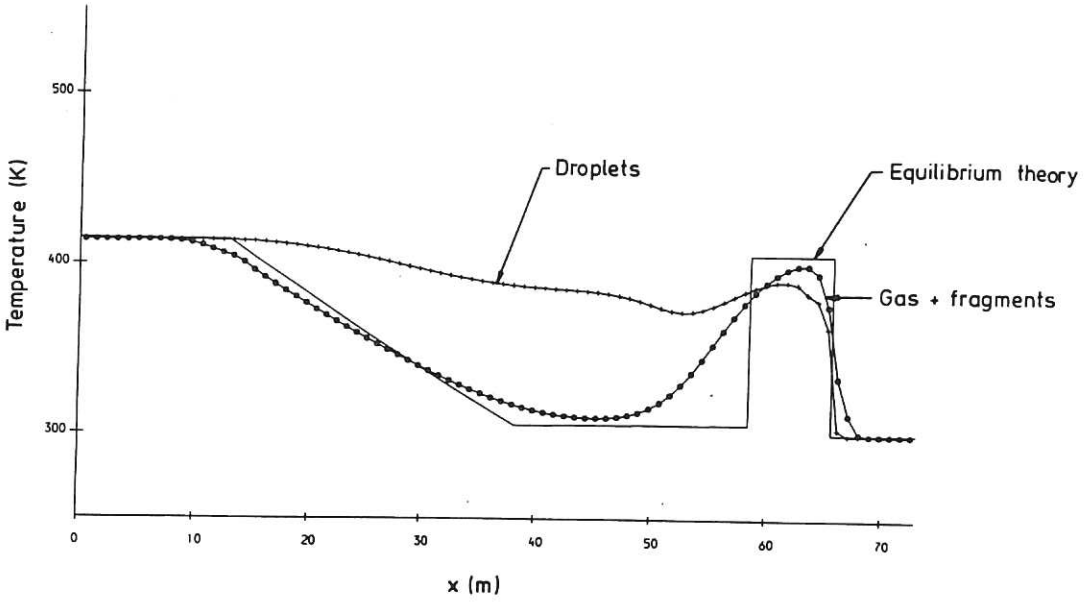

Fig.5(c): Temperature against distance for boundary layer stripping case

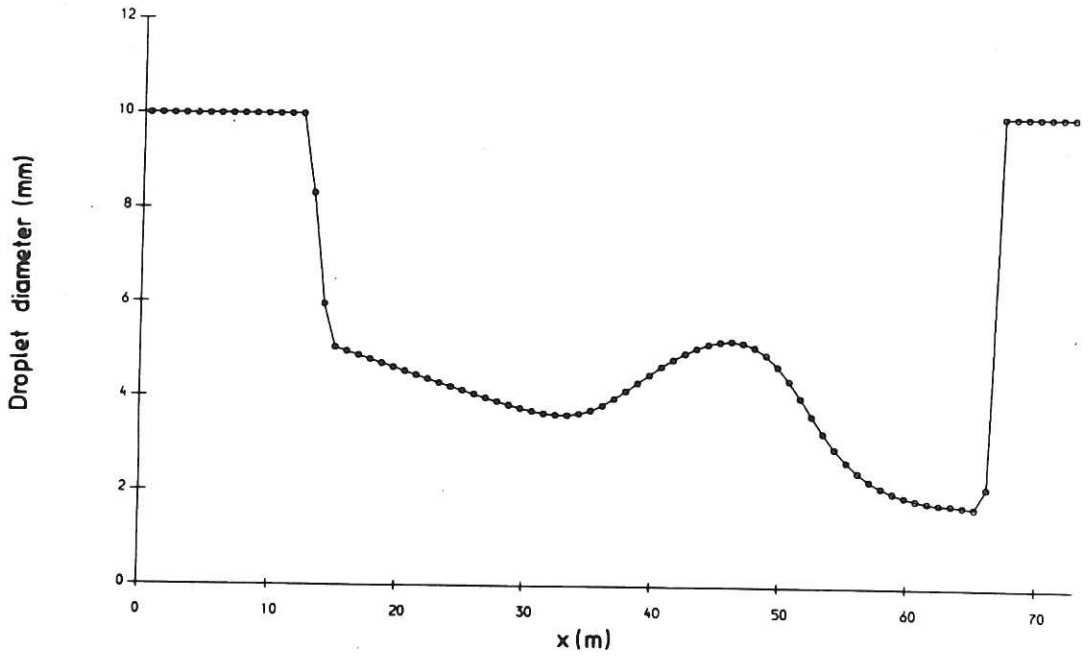

Fig.5(d): Droplet diameter against distance for boundary layer stripping case

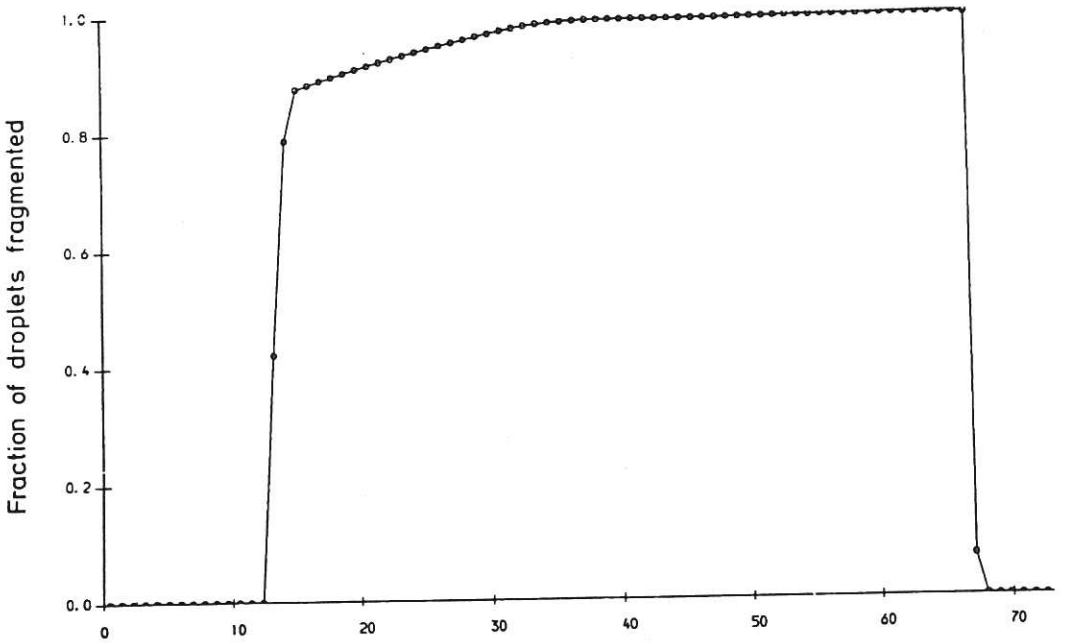

Fig.5(e): Fraction of droplets fragmented against distance for boundary layer stripping case

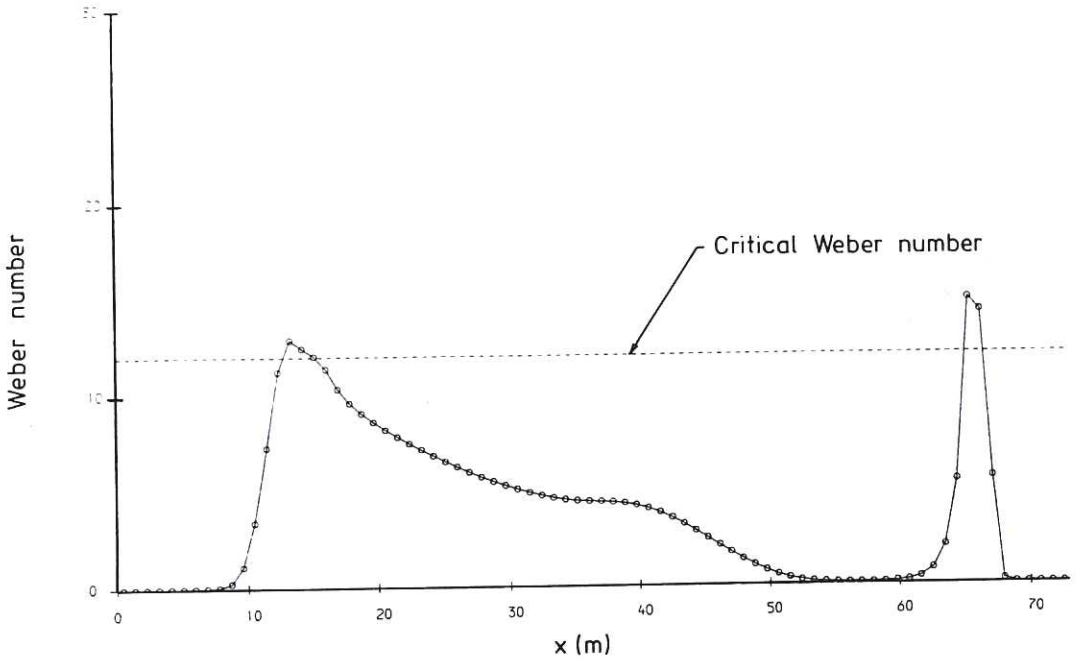

Fig.5(f): Weber number against distance for boundary layer stripping case

Available from
HER MAJESTY'S STATIONERY OFFICE
49 High Holborn, London, WC1V 6HB
(Personal callers only)
P. O. Box 276, London, SE1 9NH
(Trade orders by post)
13a Castle Street, Edinburgh, EH2 3AR
41 The Hayes, Cardiff, CF1 1JW
Princess Street, Manchester, M60 8AS
Southey House, Wine Street, Bristol, BS1 2BQ
258 Broad Street, Birmingham, B1 2HE
80 Chichester Street, Belfast, BT1 4JY

PRINTED IN ENGLAND